NeuroImage 257 (2022) 119336

Contents lists available at ScienceDirect

NeuroImage

journal homepage: www.elsevier.com/locate/neuroimage

Cross-dimensional interference between time and distance during spatial navigation is mediated by speed representations in intraparietal sulcus and area hMT+

Martin Riemer[a,b,c,d,†,*], Johannes Achtzehn[a,b,†], Esther Kuehn[b,c], Thomas Wolbers[a,c]

[a] Aging & Cognition Research Group, German Center for Neurodegenerative Diseases (DZNE), 39120 Magdeburg, Germany
[b] Medical Faculty, Otto-von-Guericke University, 39106 Magdeburg, Germany
[c] Center for Behavioral Brain Sciences (CBBS), 39106 Magdeburg, Germany
[d] Biological Psychology and Neuroergonomics, Technical University Berlin, 10623 Berlin, Germany

ARTICLE INFO

Keywords:
Cross-dimensional interference
Time-space interaction
RSA
fMRI
Intraparietal sulcus
hMT+

ABSTRACT

When navigating a straight path, perceived travel time and perceived traveled distance are linked via movement speed. Behavioral studies have revealed systematic interferences between the perception of travel time and distance, but the role of neuronal representations of movement speed for these effects has not been addressed to date. Using a combined fMRI-behavioral paradigm, we investigate the neuronal representations that underlie cross-dimensional interferences between travel time and traveled distance. Participants underwent fMRI while experiencing visual forward movements for either a short or a long duration, and covering either a short or a long distance. At the behavioral level, we found bi-directional interference effects between time and distance perception, which was correlated with greater representational similarity in speed-sensitive brain regions. The strength of the distance-on-time effect scaled with representational similarity in the left human middle temporal complex (hMT+), and the strength of the time-on-distance effect scaled with representational similarity in the right intraparietal sulcus (IPS). In accordance with the idea that the interference is mediated by the perception of speed, distance-on-time and time-on-distance effects were of opposing directions. Increases in traveled distance led to increases in perceived travel time, while increases in travel time led to decreases in perceived traveled distance. Together, these findings support the view that cross-dimensional interference effects between travel time and traveled distance are mediated by neuronal representations of movement speed.

1. Introduction

Keeping track of our location in space requires either landmark navigation or path integration (Taube, 2007). While landmark navigation is based on allothetic cues and positional information relative to salient reference points, path integration is accomplished by monitoring idiothetic self-motion cues that are independent from specific landmarks (Bremmer and Lappe, 1999; Riemer et al., 2014; Robinson and Wiener, 2021). One important idiothetic cue is the processing of visual optic flow in parietal brain regions (Britten, 2008; Martinez-Trujillo et al., 2007; Siegel, 1997) and the human middle temporal complex (hMT+; Duffy and Wurtz, 1997; He et al., 1998; Martinez-Trujillo et al., 2005, 2007; Wurtz, 1998), and neuroimaging studies have indeed reported a recruitment of these structures during visual path integration (Chrastil et al., 2015; Wolbers et al., 2007).

When we move through an environment, visual optic flow informs about both the direction and the speed of motion. The latter can be used to derive information about the distance traveled within a specific time interval and the time required to travel a specific distance. Although traveled distance and travel time are theoretically independent (the same distance can be traveled in either a short or a long time interval), an asymmetric interference between these magnitudes has often been reported: The same travel time appears longer when the associated distance is longer, while longer travel times do not result in the perception of longer distances (Cohen et al., 1963; Herman et al., 1984; Montello, 1997; Riemer et al., 2018; van Rijn, 2014). Frenz & Lappe (2005) even reported decreasing distance estimates for increasing travel times. However, while the interference between travel time and traveled distance is well documented at the behavioural level, its neuronal basis is unknown to date. A better understanding of the neuronal

* Corresponding author.
E-mail address: martin.riemer@tu-berlin.de (M. Riemer).
† shared first authorship

https://doi.org/10.1016/j.neuroimage.2022.119336.
Received 15 March 2022; Received in revised form 8 May 2022; Accepted 24 May 2022
Available online 26 May 2022.

mechanisms underlying these interference effects can provide insights into characteristic deviations, as for example occurring in advanced age or during neurodegenerative diseases where uncertainties in estimated time and distance frequently occur (e.g., Kuehn et al., 2018; Maaß et al., 2022; Mioni et al., 2021; Riemer et al., 2021; Stangl et al., 2020).

A potential neuronal mechanism for the interference between travel time and traveled distance consists in the processing of speed, because both time and distance judgments can be solved on the basis of speed representations, combined with information about the respective other dimension. If the perceptual interference between time and distance originates from common neuronal representations of speed, this should be reflected in high representational similarity during time and distance judgments in speed-sensitive brain regions, such as area hMT+ and posterior parietal regions (Britten, 2008; Duffy and Wurtz, 1997; Martinez-Trujillo et al., 2007; Wurtz, 1998).

To test whether behavioural interferences between travel time and traveled distance are associated with common representations of speed, we compared the interference between time and distance with the interference between each of these magnitudes and numerosity (i.e., the amount of dots randomly appearing along a path during visual forward motion). Twenty-five participants underwent fMRI scanning while experiencing visual forward motion along a virtual linear track, with their attention being directed either to the duration of the forward movement, the traversed distance, or the number of events encountered during the movement. To eliminate confounds driven by sensory differences, visual stimuli were identical across all conditions. We employed an adaptive design and tested all participants around their individual 50% performance threshold in each task, thereby controlling for confounds of task difficulty (Livesey et al., 2007; Tregellas et al., 2006). Finally, we controlled for stimulus repetition and adaptation effects by using a specific randomization sequence (Aguirre, 2007).

Representational similarity analysis (RSA) served to investigate the neuronal basis for the perceptual interference between travel time and traveled distance in the human brain. Specifically, if cross-dimensional interference at the behavioral level between time and distance is mediated by common neuronal representations of speed, interference should be larger when representational similarity in speed-sensitive areas is high. To the best of our knowledge, this is the first study that used a combined fMRI-behavioral paradigm to systematically investigate the neuronal mechanisms that underlie perceptual interference effects between travel time and traveled distance.

2. Materials and methods

2.1. Participants

Twenty-five right-handed participants were recruited from the local community (14 females and 11 males, mean age: 24.9 years, ranging from 20 to 41 years). Required sample size of 22 ($\alpha = 0.05$; $1\text{-}\beta = 0.80$) was calculated with G*Power (Faul et al., 2007), based on effect sizes reported in Riemer et al. (2018). Exclusion criteria were contraindications to magnetic resonance imaging, such as metallic objects in the body, or tinnitus. The data of one participant were excluded from the analysis due to missed responses in more than 20% of the trials, casting doubt on overall attention. All participants received monetary compensation and gave written informed consent to the experimental protocol, which was approved by the local ethics committee of the University of Magdeburg.

2.2. Experimental design

2.2.1. Stimuli, tasks and trial order

In a path integration paradigm we probed cross-dimensional interferences between travel time and traveled distance, and compared them to the interference between each of these magnitudes and numerosity (the amount of items encountered during walking). In our experimental design, visual input was identical between the tested dimensions, that is, participants always saw a virtual linear track projected onto a screen along which they were passively moved forward (see Fig. 1). Optic flow information was provided by the textures of the track and the grassy landscape alongside. To prevent participants from fixating specific locations at the far end of the track (and instead force them to continuously integrate the accumulating distance information), viewing distance was limited by gray fog that linearly increased in density, starting one meter in front of the participant. In different experimental conditions, only the instruction varied, indicating to the participant which one of four dimensions (i.e., time, distance, numerosity, luminance) they had to attend to in each trial. Numerosity trials served as a control condition involving an accumulation process for a different magnitude (i.e., numerosity). Luminance trials were chosen as a control condition involving only the decision component, in which the critical dimension (i.e., luminance) did not accumulate over the course of the trial.

In each trial, one of four task symbols (i.e., time, distance, numerosity or luminance) was presented for 500 ms (see Fig. 1). After an interstimulus-interval (ISI; randomised between 2 and 3 s), during which a blank screen was shown, a path was displayed and the observer was passively moved forward. Movement speed varied between trials, but was kept constant within each trial. Across trials, the covered distance was either 11.5 or 19.7 m (distance), and the travel time was either 2.8 or 4.8 s (time). During the forward motion, either 45 or 77 white dots (numerosity) flashed on the path. The dots did not flash all at once but in an irregular manner, so that their total sum accumulated until the end of the forward motion. 200 ms before the forward motion was terminated by a black screen, a gray square of either 16 or 28 pct white content (luminance) appeared in the middle of the screen. All levels of these four dimensions were combined equally with each other, resulting in 16 different combinations. After an ISI of 1 s, a comparison number was displayed on the screen and the participants had to perform a two-alternative forced-choice task. In time trials, participants indicated via button press whether the travel time was shorter or longer than this comparison number in seconds. In distance trials, they indicated whether the traveled distance was shorter or longer than this comparison number in meters. In numerosity trials, they indicated whether the number of flashed dots was smaller or larger than this comparison number. Comparison numbers were integers in numerosity trials and had one decimal during time and distance trials. Finally, in luminance trials, the comparison value consisted of a displayed square with variable white content, and participants indicated whether the square presented at the end of the forward motion was darker or brighter than this comparison square.

Responses were given with the index finger (‘less’) or the middle finger (‘more’) of the right hand, and participants had 2 s time to respond. If no response was given within this time window, a message ‘Please respond faster!’ was displayed in red letters for 0.5 s. Participants had the option to indicate that they had forgotten the cue (indicating the relevant dimension for the current trial) by pressing the thumb key. No feedback was provided throughout the whole experiment.

The experiment was composed of four different trial types (each presented 100 times) plus 100 null trials, in which a fixation cross was presented on a gray background. To account for possible repetition effects, all trials were ordered according to a continuous carryover sequence (Aguirre, 2007). This second-order counterbalanced sequence ensured that each trial type (including null trials) was preceded by every other trial type (including itself) for an equal number of times. One de Bruijn sequence balancing five conditions at the second order included 125 trials. This sequence was split in half (i.e., 63 and 62 trials) and distributed over two separate scan runs. To retain the circularity of de Bruijn sequences, the final two trials of each run were added to the start of the corresponding run, resulting in 65 or 64 trials per run (cf. Fig. 1C).

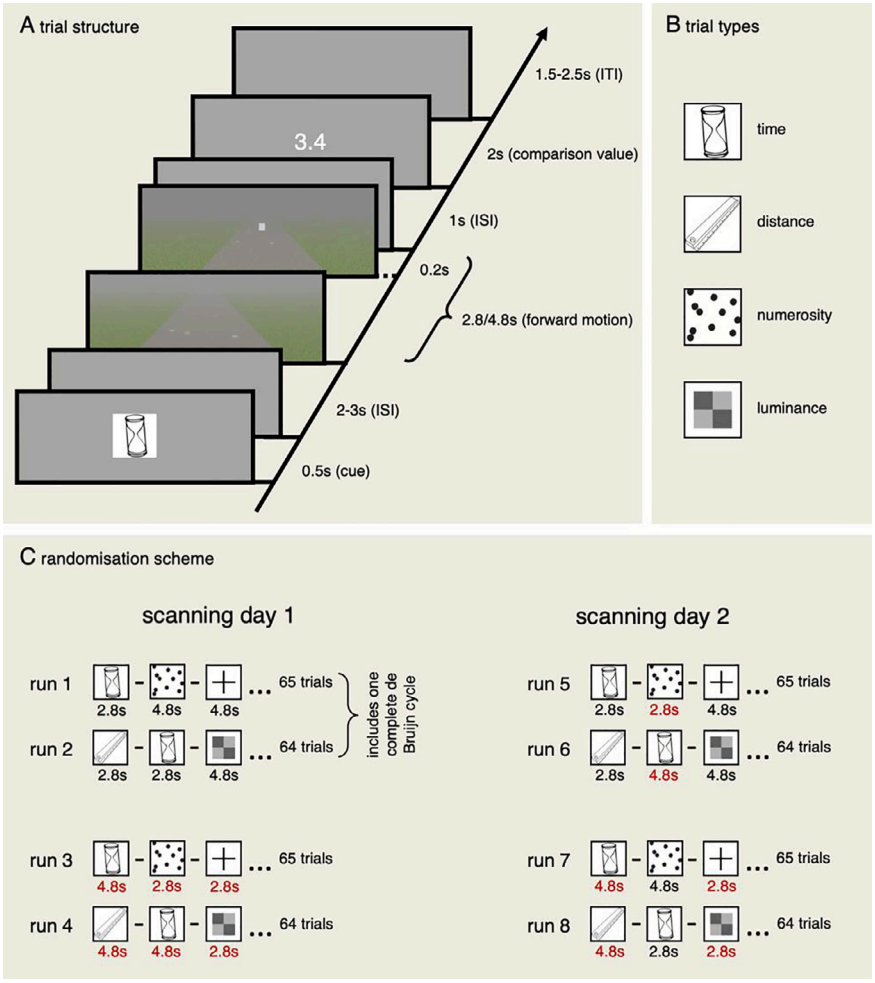

Fig. 1. Experimental design. (A) Each trial began with the presentation of a cue, which informed participants about the dimension (time, distance, numerosity, luminance) they had to attend to. Next, a gray linear track surrounded by green grass was shown, and the observer experienced a passive forward movement along the path. The covered distance was either 11.5 or 19.7 m, travel time was either 2.8 or 4.8 s, and either 45 or 77 white dots appeared on the ground. During the last 200 ms of each forward motion, a gray square of either 16 or 28 pct white content appeared on the screen. Once the forward motion had ended, participants had to judge whether the magnitude in question was smaller or larger than a presented comparison value. **(B)** The four symbols used to inform participants about the trial type at the start of each trial. **(C)** The task was performed in eight runs, on two different days. Two subsequent runs comprised a complete de Bruijn sequence (5^3=125 elements), which was equal for all four runpairs. Relative to the original sequence in run 1–2, the level of travel time (short/long) was switched for all trials in run 3–4, for even trials in run 5–6, and for odd trials in run 7–8 (indicated by red numbers).

Furthermore, we balanced the trials with respect to (short and long) travel times, because those differed in their total duration (10.8 and 12.8 s).[1] This was achieved by repeating the two runs (containing one complete de Bruijn sequence) four times. In the first repetition, short and long trials were inverted (i.e., each short trial from the original sequence was changed to a long trial and vice versa). In the second repetition, only even trials from the original sequence were inverted, and in the third repetition, only odd trials were inverted. This procedure ensured that the order of short and long trials was balanced. The resulting eight runs were conducted in two separate sessions on two different testing days (maximally one month apart). Each session lasted about 75 min.

2.2.2. Task difficulty

To maintain comparable levels of task difficulty across the four tasks for each participant, and over the course of the experiment, an adaptive procedure was employed when selecting comparison numbers (or, in luminance trials, the white content of the comparison square): Depending on the response ('less' or 'more') in the previous trial involving the same standard (e.g., a time trial with 4.8 s), the new comparison value was randomly chosen from a range of zero to $\frac{1}{4}$ times below or above this previous value, respectively. The first comparison value was randomly chosen between $\frac{1}{4}$ times below to $\frac{1}{4}$ times above the respective standard value.

Finally, after each run, participants rated the difficulty of the four different tasks on a visual analogue scale (balanced order) via button press. Participants used the index and middle finger keys to move a marker along an easy-difficult continuum and confirmed their response with the thumb key.

2.3. Acquisition of fMRI data

MRI data were acquired on a 3T Siemens Magnetom Prisma scanner, equipped with a 64-channel phased array head coil. Functional images were recorded with an echo-planar-imaging (EPI) sequence (TR = 2000 ms; TE = 30 ms; slice thickness = 3 mm; voxel size = 3 × 3 × 3 mm; number of slices = 36; field of view = 216 mm; flip angle = 90°; slice acquisition order = interleaved). Anatomical data consisted of (i) a T1-weighted image (MPRAGE, TR = 2500 ms; TE = 2.82 ms; TI = 1100 ms; slice thickness = 1 mm; number of slices = 192; voxel size = 1 × 1 × 1 mm; field of view = 256 mm; flip angle = 7°), as well as (ii) a T2-weighted image (TSE, TR = 6000 ms, TE = 73 ms, slice thickness = 2 mm, number of slices = 60, voxel size = 2 × 2 × 2 mm, field of view = 512 mm, flip angle = 120°). Additionally, in each session, double-echo gradient-echo field maps were calculated (echo times 4.92 ms and 7.38 ms). Each run took approximately 15 min to complete.

2.4. Preprocessing of fMRI data

Anatomical and functional images were preprocessed using fMRIPrep 1.1.1 (Esteban et al., 2019). In this pipeline, T1/T2 weighted (T1w/T2w) images were corrected for intensity non-uniformity with ANTs' N4BiasFieldCorrection v2.1.0 (Tustison et al., 2010). Afterwards, they were skull-stripped using ANTs' antsBrainExtraction.sh v2.1.0 (OA-

[1] Although ISIs between cue and passive forward motion were jittered, the temporal differences were compensated for during the ITIs, so that each trial was either 10.8 s or 12.8 s in duration.

SIS template; Marcus et al., 2007) to create an initial binary mask of the brain. After brain mask computation, FSL FAST v5.0.9 (Zhang et al., 2001) was used to perform brain tissue segmentation (CBF, white matter, gray matter). Brain surface reconstruction was performed by recon-all from FreeSurfer v6.0.1 (Dale et al., 1999). The initial brain mask was refined with a fMRIPrep custom variation of the method to reconcile ANTs-derived and FreeSurfer-derived segmentations of the cortical gray-matter (Klein et al., 2017). In the last step, spatial normalization to the MNI152NLin2009cAsym template space (Fonov et al., 2009) was performed using antsRegistration. This entails a multiscale, mutual-information based, nonlinear registration scheme.

During the initial step of BOLD image preprocessing, a reference image was created in order to calculate a brain mask for the BOLD signal.[2] This EPI reference image was then passed to FSL's mcflirt v5.0.9 (Jenkinson et al., 2002) in order to estimate head motion parameters (three for rotation and three for translation). Slice time correction was performed using AFNI v16.2.07 3dTShift function (Cox, 1996), realigning each slice to the middle of each TR. Next, spatial distortion due to B0 field inhomogeneities were accounted for by susceptibility distortion correction (SDC) using an implementation of the TOPUP technique (Andersson et al., 2003) using function 3qwarp in AFNI v16.2.07. Hereby, the field inhomogeneity can be mapped by measuring the phase evolution in time between two close GRE acquisitions (Hutton et al., 2002). Finally, the BOLD reference image was aligned to the T1w image using linear boundary-based registration with 9 DOF implemented in FSL flirt. To map the EPI image to the MNI152NLin2009cAsym template space, transform calculated upstream (head-motion estimation, SDC, EPI to T1w registration, T1w-to-MNI transform) workflows are concatenated. These transforms are applied all at once with one Lanczos interpolation step.

2.5. Statistical analysis of behavioral data

Trials with response times shorter than 300 ms (0.2%) or longer than 2 s (2.7%)[3] after the onset of the comparison value were discarded for behavioral analyses. In the luminance task, three participants confused the meaning of response buttons ('less' vs. 'more') in the first fMRI session. The corresponding behavioral data were removed.

Effects on difficulty ratings and reaction times were tested by analyses of variance (R function *aov* from package *stats*), including the within-subjects factors trial type (time vs. distance vs. numerosity vs. luminance) and run number (1–8). If relevant, pairwise post-hoc comparisons were performed with *Tukey's HSD* test.

After a manipulation check with one-tailed t-tests, confirming that participants were able to differentiate between the small and the large standard value of each dimension (e.g., short and long travel times), analyses were performed on the ratios between comparison and standard value. This allowed for a conjoint analysis of responses to both small and large standards.

For each participant and each dimension, one psychometric function was calculated using the Bayesian-based toolbox psignifit 4 (Schütt et al., 2016). This toolbox was chosen because (i) it is robust against (potentially) overdispersed data, (ii) accounts for sparse and varying trial numbers per sampled intensity, (iii) allows for a transparent adjustment of parameters, and (iv) provides a reliable proxy for the goodness-of-fit. Default priors were adjusted according to the expected range of the behavioral data, given the adaptive approach of defining the comparison value for each trial. Specifically, the prior **w** for the width of the psychometric function was increased to a uniform distribution between four times the minimal distances between two stimulus intensities (lower limit) and three times the total range of stimulus intensities (upper limit) with a cosine fall-off to 0 at both ends. The lapse rate was fixed at λ=0.01. Preliminary analyses of the data showed that a variable lapse rate with a beta-distributed prior resulted in overestimated lapse rates due to the low number of trials for some comparison values, especially near the lower and upper intensity boundaries. All other priors (e.g., threshold and guess rate) were left at their default settings.

Fitted psychometric functions represent the probability of the response 'comparison value was larger than the experienced standard value', as a function of the (standardised) comparison value (cf. Fig. 2a). Mean accuracy and precision were quantified by the point of subjective equality (PSE) and the width of the psychometric function, respectively. If two magnitudes are processed by the same neuronal mechanism, precision for those magnitudes should be positively correlated. This was tested by correlation analyses (one-tailed). Direct comparison between correlation coefficients was performed with R function *paired.r* from package *psych*.

For the analysis of cross-dimensional interference effects, we separately calculated psychometric functions for each dimension using only trials associated with either the small or the large standard of the irrelevant dimension (e.g., travel distance during time trials). For example, to investigate the influence of traveled distance on perceived time, one function for time judgments was calculated on the basis of time trials involving a short travel distance, and a second one based on time trials involving a long travel distance (see Fig. 2C). Cross-dimensional interference effects were quantified by the PSE difference between these two functions, so that positive values indicate congruent interference (i.e., larger values of the irrelevant dimension led to an overestimation of the target dimension). Values deviating more than three standard deviations from the mean were discarded as outliers (0.7%). Cross-dimensional interference effects were analysed with t-tests (two-tailed). The relationship between interference effects and representational similarity (see Section 2.6.2) was tested by Spearman rank correlations (two-tailed).

Effect sizes are reported by means of partial eta squared (η_p^2) for anovas and Cohen's d_{av} for t-tests (Lakens, 2013).

2.6. Statistical analysis of fMRI data

2.6.1. Univariate analysis

Design and implementation of the univariate analysis was done using the nipype v1.5.1 Python framework (Gorgolewski et al., 2011), which allows for a flexible and accessible implementation of multiple neuroscientific software packages in one workflow. SPM12 v7487 MATLAB 2016b (The MathWorks, Natick, 2016) was utilised for model generation and contrast estimation. The functional images were smoothed using a 6 mm FWHM Gaussian filter and masked with an individual brain mask obtained from fMRIPrep using the extractroi function of FSL. The data were high-pass filtered at 128 Hz. Trials of interest were modeled as delta functions (covering the entire period of movement, i.e., either 2.8 or 4.8 s) that were convolved with the hemodynamic response function as implemented in SPM12. Additionally, the cue and the comparison phase (until a response was given, maximally 2 s; cf. Fig. 1) were included as regressors. As nuisance regressors, six head motion parameters and framewise displacement were included. In addition to computing the contrasts "time>control", "distance>control" and "numerosity>control", we also performed a conjunction analysis for these contrasts. For the second level, classical inference with one sample t-tests were performed on all contrasts. Threshold criteria were a voxel-wise FWE (p<.05) and a minimum cluster size of 10 voxels. As reported in Eklund et al. (2016), this approach tends to be conservative, but avoids the inflated false-positive bias of the clusterwise FWE. The anatomical location of each cluster was assessed by the JuBrain Anatomy v3.0 SPM Toolbox (Amunts et al., 2007; Eickhoff et al., 2005). Unless otherwise specified, reported coordinates in MNI space represent location of peak voxels in the respective cluster.

[2] Please see Esteban et al. (2019) for a detailed explanation of the employed steps.

[3] Note that this also includes cases in which the participant forgot the cue and withheld a response on purpose.

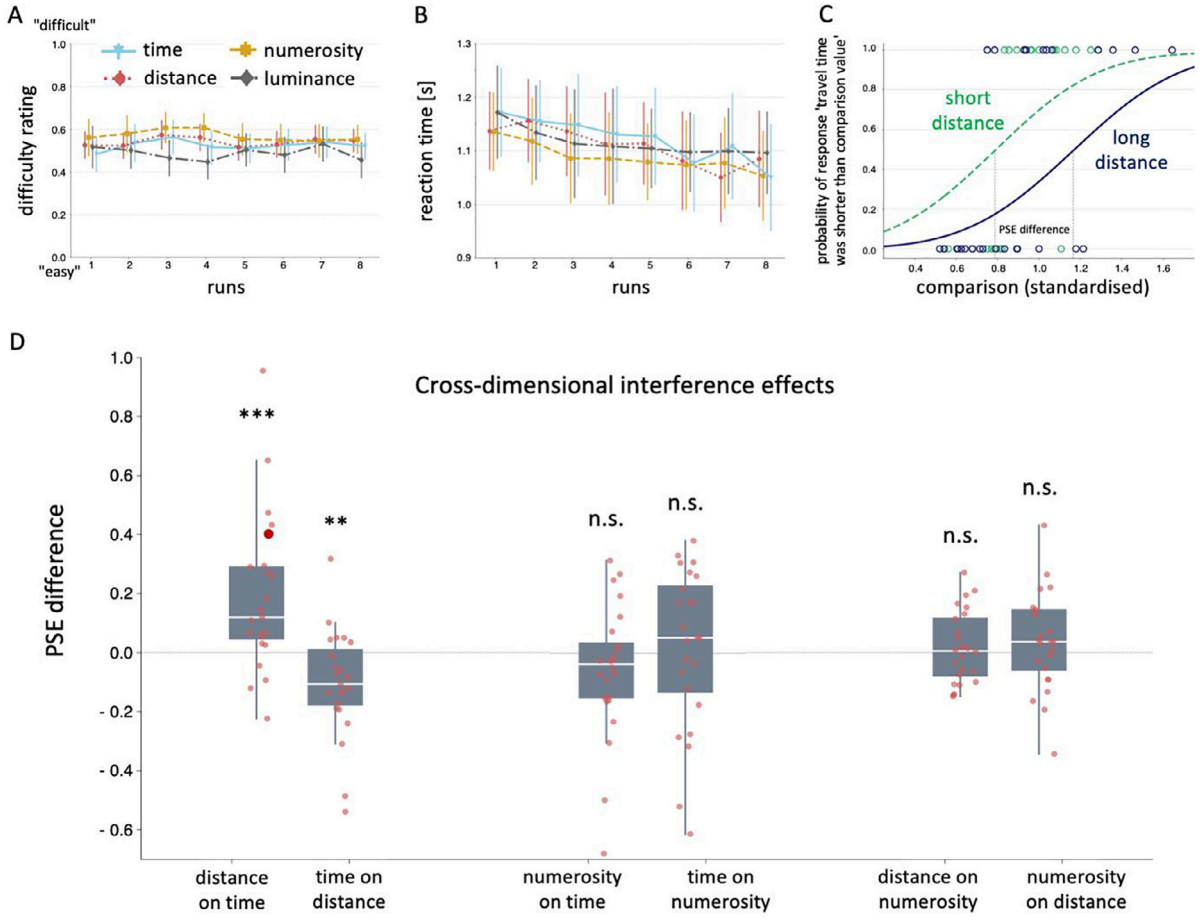

Fig. 2. Behavioral results. (A) Subjectively perceived difficulty and **(B)** reaction times for time (blue), distance (red), numerosity (yellow) and luminance/control trials (black) over the course of eight runs. Difficulty was rated after each run on a visual analogue scale. Error bars show standard error across subjects. **(C)** Cross-dimensional effect of distance on time judgments, exemplary for one subject. Even though travel distance was irrelevant for time judgments, travel time was judged as shorter for trials with a short travel distance (dashed line) as compared to trials with a long travel distance (solid line). **(D)** Cross-dimensional interference effects between time, distance and numerosity ($^{***}p<.001$; $^{**}p<.01$; $^{n.s.}p>.05$). Boxes show median (white lines) and interquartile ranges (box span). The bold point in the distance-on-time effect indicates the exemplary subject shown in **C**.

2.6.2. Representational similarity analysis

To investigate the relation between representational similarity at the neuronal level and cross-dimensional interference on the behavioral level, we performed a whole-brain searchlight representational similarity analysis (RSA) and correlated the resulting voxel-wise representational dissimilarity values (RDVs) for each possible dimension pair (time-distance, distance-numerosity, time-numerosity) with the individual cross-dimensional interference effects. The RSA was based on Pearson correlation distance and a whole-brain searchlight with a radius of 6 mm together with a leave-one-run-out cross validation scheme (Walther et al., 2016). Because such analyses are prone to inflated correlations due to a nonindependence error (Vul et al., 2009), we split the available eight runs in odd and even runs. Data from the odd runs were used to create masks containing only voxels that show significant Spearman rank correlation coefficients ($p<.05$). Additionally, a cluster-threshold of $k = 10$ voxels was applied.[4] The actual Spearman rank correlation coefficients (two-tailed), based on data from the even runs, were then computed only for the voxels of the mask obtained from analysing the odd runs. This resulted in three R-maps, in which each voxel carries the Spearman rank correlation coefficient (and corresponding p-value) between RDVs and cross-dimensional interference. As for the univariate analysis, JuBrain Anatomy v3.0 SPM Toolbox was used to characterize cluster locations (Amunts et al., 2007; Eickhoff et al., 2005).

In a second analysis, we quantified representational similarity between time, distance and numerosity in regions with significant activation for either of the three dimensions in the univariate analysis. RDMs for all clusters were calculated separately, again using Pearson correlation distance and a leave-one-run-out approach. For this analysis, two successive runs were grouped together (as they encompass one complete de Bruijn sequence; cf. Section 2.2.1), resulting in a 4-fold cross validation scheme. T-tests to compare representational similarity between different dimension pairs were two-tailed and corrected for multiple comparisons according to the false discovery rate (Benjamini and Hochberg, 1995).

All RSA calculations were performed within the PyMVPA2 framework (Hanke et al., 2009). As input data, trial-wise beta estimates were calculated. These were obtained by computing a GLM for each trial in which the specific trial is modeled as the regressor of interest. All other occurrences of that specific trial type during the run as well as the trials of different types were modeled in separate nuisance regressors. This approach (named "LS2") was found to be superior in classification performance for rapid event-related designs compared to modeling each trial as a separate regressor (Mumford et al., 2012; Turner et al., 2012). Except for the included regressors, this analysis was performed

[4] To test whether this cluster-threshold was too conservative, we ran an additional analysis with k = 5. This did not reveal different results. Details for this analysis can be found at https://github.com/jAchtzehn/timePath/tree/wholeBrain-CV/mri/rsa.

with the same software and parameters as the univariate analysis (cf. Section 2.6.1).

3. Results

3.1. Behavioral results

3.1.1. Task difficulty and reaction times

As shown in Fig. 2A, perceived difficulty differed between time, distance, numerosity and luminance trials ($F_{3,748}$=7.6, p<.001, η_p^2=0.03), but did not change over the course of the eight runs ($F_{1,748}$<0.1, p>.5, η_p^2<0.01). There was also no interaction between trial type and runs ($F_{3,748}$=0.4, p>.5, η_p^2<0.01). A pairwise post-hoc *Tukey's HSD* test revealed that the effect of trial type was due to luminance trials being rated as easier than time trials (diff=0.06, p_{adj}=0.019, d_{av}=0.29), distance trials (diff=0.07, p_{adj}=0.003, d_{av}=0.38), and numerosity trials (diff=0.09, p_{adj}<0.001, d_{av}=0.42). Differences between time, distance and numerosity trials did not reach a significant level (all: diff<0.03, p_{adj}>0.32, d_{av}<0.17). This demonstrates that the adaptive procedure for the selection of comparison values was effective in keeping perceived difficulty for time, distance and numerosity trials at a comparable level.

In line with this interpretation, Fig. 2B shows that reaction times did not differ between trial types ($F_{3,748}$=0.8, p=.48, η_p^2<0.01). Reaction times decreased over the course of the experimental runs ($F_{1,748}$=11.9, p<.001, η_p^2=0.02), but did not change differently depending on trial type ($F_{3,748}$=0.2, p>.5, η_p^2<0.01).

3.1.2. Judgment precision and cross-dimensional interference

We first tested whether participants were able to differentiate between the small and the large value of each dimension. One-tailed t-tests for paired samples confirmed that the PSE was significantly larger for the large as compared to the small standard value for time (t_{23}=8.0, p<.001, d_{av}=1.15), distance (t_{23}=4.7, p<.001, d_{av}=1.38), numerosity (t_{23}=9.6, p<.001, d_{av}=1.23), and luminance (t_{23}=9.5, p<.001, d_{av}=3.33). To confirm that time, distance and numerosity trials were based on accumulation processes, we tested whether precision (cf. Section 2.5) decreased with increasing magnitude (due to the accumulation of noise). This was confirmed for time (t_{23}=2.0, p=.028, d_{av}=0.53), distance (t_{23}=2.3, p=.014, d_{av}=0.60) and numerosity trials (t_{23}=3.6, p<.001, d_{av}=0.55), but not for luminance/control trials (t_{23}=1.6, p=.06, d_{av}=0.45).

Judgment precision was correlated between time and distance trials (t_{22}=2.0, p=.030, r = 0.39), demonstrating that individuals who were relatively precise in their time judgments also tended to be relatively more precise in their distance judgments. In contrast, correlations were neither found between the precision in time and numerosity trials (t_{22}=1.2, p=.13, r = 0.24) nor between distance and numerosity trials (t_{22}=−0.1, p>.5, |r|<0.1). However, a direct comparison between correlation coefficients showed that the correlation between time and distance trials was significantly different only from the correlation between distance and numerosity trials (p=.05), but not from the correlation between time and numerosity trials (p=.31).

With respect to cross-dimensional interferences (Fig. 2C-D), two-tailed t-tests revealed that perceived travel time was influenced by traveled distance (t_{23}=3.7, p=.001, d_{av}=0.53), but not by numerosity (t_{23}=−1.3, p=.21, d_{av}=0.16). Perceived traveled distance was influenced by travel time (t_{22}=−2.8, p=.011, d_{av}=0.36), but not by numerosity (t_{23}=1.4, p=.19, d_{av}=0.19). And perceived numerosity was neither influenced by travel time (t_{23}=0.3, p>.5, d_{av}=0.06) nor by traveled distance (t_{23}=0.7, p>.5, d_{av}=0.07). Direct comparisons confirmed that perceived travel time was influenced more by travel distance than by numerosity (t_{23}=3.6, p=.001), that perceived traveled distance was influenced more by travel time than by numerosity (t_{22}=−2.8, p=.011), and that the influence on perceived numerosity was not significantly different for travel time and traveled distance ($|t_{23}|$=<0.1, p>.5).

Importantly, the effects of time-on-distance and distance-on-time were of opposing directions: Longer travel distances resulted in longer time judgments, whereas longer travel times resulted in shorter distance judgments (t_{22}=5.0, p<.001).

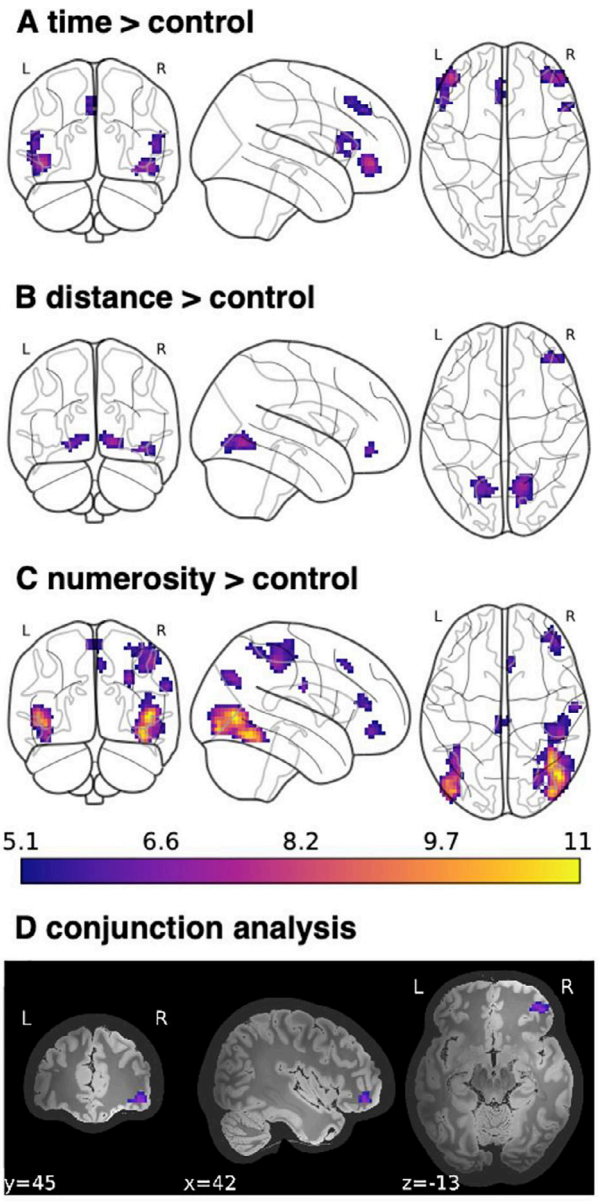

Fig. 3. Univariate fMRI results. Contrasts for **(A-C)** accumulation (time, distance and numerosity) vs. control (luminance) trials, and **(D)** results of a conjunction analysis for these three contrasts. Cluster size > 10 voxels, T = 5.12 (p = .05; FWE-corr). For specifications of brain regions see Table 1.

3.2. fMRI results

3.2.1. Overlapping brain activations for the processing of time, distance and numerosity

First, we contrasted time, distance and numerosity trials with luminance trials (as they did not involve an accumulation process), to identify areas involved in the accumulation of those quantities (Fig. 3A-C and Table 1). For time trials, recruited areas comprised the pars orbitalis of the inferior frontal gyrus (IFG) bilaterally and the left superior frontal gyrus. For distance trials, the right IFG (pars orbitalis) and the lingual gyrus bilaterally were involved. For numerosity trials, recruited areas consisted of the right IFG (pars orbitalis), right parietal lobe (including the IPS), area hMT+ bilaterally, and the right superior frontal gyrus. A conjunction analysis combining these three contrasts revealed the right

Table 1
Univariate fMRI results. Significant clusters identified for **(A-C)** accumulation (time, distance and numerosity) vs. control (luminance) trials, and **(D)** conjunction analysis. Coordinates represent the peak of the activated cluster.

Region	MNIcoordinates	Clustersize	Voxel level(T-value)
A time > control			
L inferior frontal gyrus (p. orbitalis)	−45, 45, −5	108	7.92
R inferior frontal gyrus (p. orbitalis)	42, 45, −9	90	7.25
R inferior frontal gyrus (p. opercularis)	51, 18, 11	37	6.56
L inferior frontal gyrus (p. triangularis)	−51, 33, 1	63	6.39
L superior medial gyrus	−3, 39, 41	47	6.23
B distance > control			
L lingual gyrus	−21, −66, −5	77	6.51
R lingual gyrus	15, −63, −5	122	7.39
R inferior frontal gyrus (p. orbitalis)	42, 45, −12	43	6.57
C numerosity > control			
R middle temporal gyrus (V5)	48, −69, 1	519	11.29
fusiform gyrus	42, −60, −15		10.53
inferior occipital gyrus (V4)	42, −84, −9		10.36
L middle occipital gyrus (hO4cla)	−45, −84, −2	314	9.69
inferior occipital gyrus (V4)	−39, −69, −12		7.77
fusiform gyrus	−42, −57, −15		7.45
R inferior parietal lobule	51, −36, 51	199	7.36
postcentral gyrus	42, −33, 57		6.48
superior parietal lobule	39, −48, 57		6.11
R middle occipital gyrus	30, −72, 34	51	7.09
R postcentral gyrus	63, −12, 28	21	6.71
R inferior frontal gyrus (p. orbitalis)	42, 48, −12	54	6.54
R inferior frontal gyrus	45, 42, 11	34	6.48
L paracentral lobule	−6, −30, 61	38	6.18
R posterior-medial frontal gyrus	6, 24, 47	20	6.10
D (time > control) AND (distance > control) AND (numerosity > control)			
R inferior frontal gyrus	42, 45, −12	29	6.52

IFG as the only region to be commonly activated in time, distance and numerosity trials (Fig. 3D and Table 1).

3.2.2. Correlation between cross-dimensional interference and representational similarity

Finally, we tested how the observed behavioral interference effects relate to the representational similarity of the involved neuronal networks. If the cross-dimensional interference effects that we observed between time and distance (cf. Section 3.1.2) emerge from common neuronal representations in speed-sensitive areas, greater representational similarity in these regions should coincide with more pronounced interference effects. To test this hypothesis, we performed a representational similarity analysis and assessed the correlation between the time-distance representational similarity and the behavioral measures of time-distance interference.

Results are depicted in Fig. 4. Representational similarity between time and distance was positively correlated with the cross-dimensional interference effect of distance on time (indicated by a negative correlation with representational dissimilarity) in the left fusiform gyrus and the left area hMT+ (percent of cluster volumes: 16.3% in FG4, 9.2% in hOc5 based on maximum probability map; probabilities: global maximum 64.3% in FG4, two local maxima with 49.6% and 86.3% in hOc5, respectively; Lorenz et al., 2015; Malikovic et al., 2006). In accordance with the negative interference effect of time on distance (i.e., increased travel time led to shorter distance estimates; cf. Fig. 2D), a positive correlation with representational dissimilarity was found in the right IPS (percent of cluster volumes: 75.5% in hIP3, 3.4% in hIP6 based on maximum probability map; probabilities: global maximum 49.8% in hIP3, two local maxima with 55.7% and 39.8% in hIP3; Richter et al., 2019; Scheperjans et al., 2008). Hence, for both types of interference, these correlations indicate that higher representational similarity in the respective area coincide with a larger interference effect measured in behavior.

With respect to the cross-dimensional interference between time and numerosity and between distance and numerosity, no correlations with representational similarity between the respective trials were found.

The RDMs in Fig. 4C show that representational similarity between time and distance was larger than between time and numerosity and between distance and numerosity. However, left hMT+ and right IPS were defined by their correlation with time-distance interference effects and therefore are not indicative of a generally higher representational similarity between time and distance trials. To solidify this assumption, we calculated the RDMs for all regions showing higher activity during the accumulation of either time, distance or numerosity (cf. Fig. 3A-C).

The results are presented in Fig. 5 and Table 2. For many regions, representational similarity between time and distance trials was significantly larger than between time and numerosity or distance and numerosity trials (cf. Table 2). Importantly, there was no region for which the time-distance representational similarity was smaller than that for time-numerosity or distance-numerosity. This pattern of results mirrors the behavioral cross-dimensional interference effects, which were exclusively found between time and distance (cf. Section 3.1.2).

4. Discussion

In the present study we examined the representations of travel time and traveled distance, in order to identify neuronal mechanisms underlying the perceptual interference between these dimensions. We found a mutual interference between travel time and traveled distance, but of opposing direction: Perceived travel time *increased* with longer distances, while perceived distance *decreased* with longer travel times. The strength of these interference effects was associated with greater representational similarity in speed-sensitive parietal and extrastriate brain areas. The effect of distance on time was correlated with higher representational similarity in left area hMT+, and the effect of time on distance was correlated with higher representational similarity in the right IPS. We therefore conclude that neuronal representations of movement speed in parietal and occipital regions (derived from visual optic flow) play a major role for the cross-dimensional interference between travel time and traveled distance.

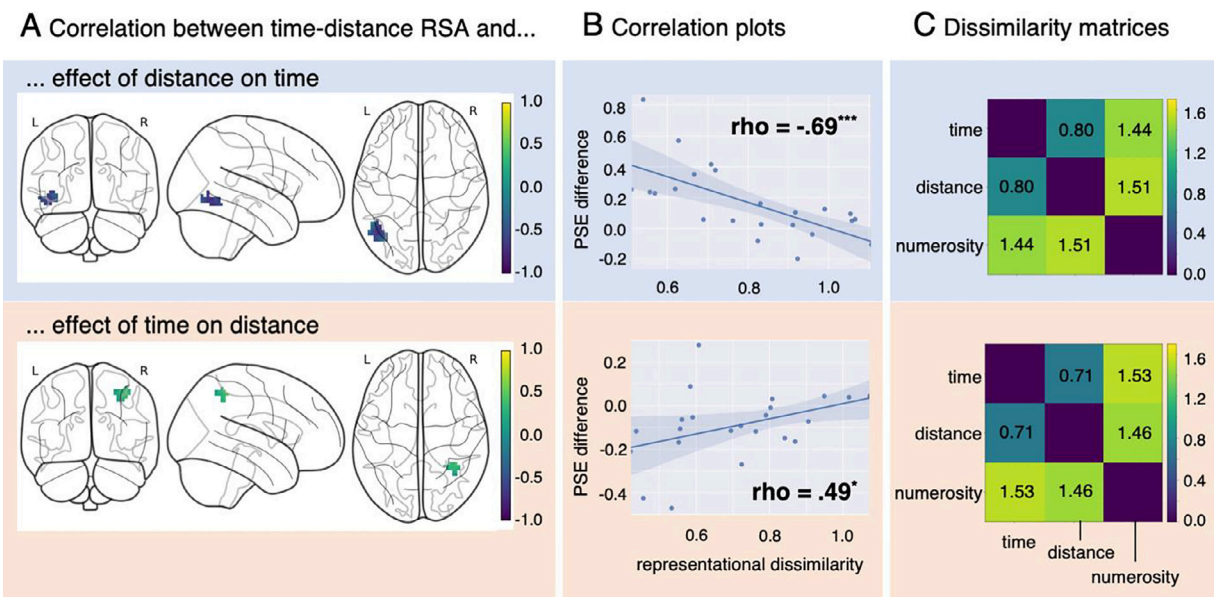

Fig. 4. Representational similarity and cross-dimensional interference. (A) R-maps showing voxels with a significant spearman rank correlation coefficient between time-distance representational similarity values and cross-dimensional interference between these dimensions. **(B)** Exemplary for the voxel with the highest absolute Spearman rank correlation coefficient, linear regression plots between PSE difference and representational dissimilarity value are plotted. For the same voxel, **(C)** shows the average representational dissimilarity matrix of all participants (left fusiform gyrus / hMT+ for distance-on-time [−45, −66, −9]; right IPS for time-on-distance [39, −45, 51]).

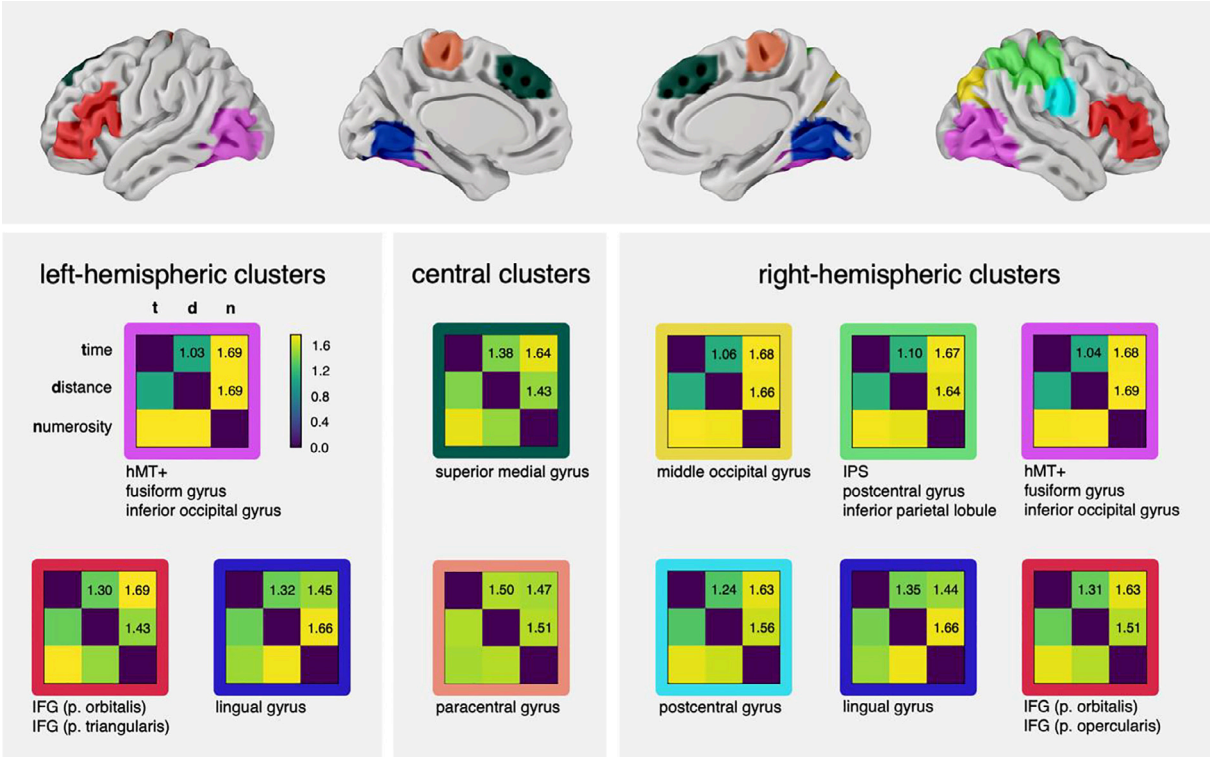

Fig. 5. RSA results. Average representational dissimilarity matrices of all participants for brain regions involved in either time, distance or numerosity accumulation (cf. Fig. 3A-C and Table 1A-C). Smaller RDM values indicate greater representational similarity. The top panel shows interpolated cortical projections of the cluster masks.

The idea that the interference between travel time and traveled distance is mediated by movement speed is also in line with our finding of an opposite direction for the distance-on-time and the time-on-distance effect (cf. Fig. 2D). One possible origin for cross-dimensional interference effects is a congruent mapping on the respective more-less continua: Larger values of the task-irrelevant dimension lead to larger estimates of the task-relevant dimension (e.g., a louder sound leads to a longer estimated duration of that sound). If the illusory increase of an actually constant travel time is driven by an increase in speed (rather than by an increase in distance), then we would still expect a positive relation between traveled distance and perceived travel time, because, given a constant travel time, distance correlates positively with speed (traveling

Table 2
RSA results. Results of two-tailed t-tests comparing representational similarity (RS) between pairs of dimensions for brain regions involved in either time, distance or numerosity accumulation (cf. Fig. 3A-C and Table 1A-C). Tests were corrected for multiple comparisons according to the false discovery rate (Benjamini and Hochberg, 1995).

Cluster (cf. Fig. 5)	Hemi-sphere	time-distance RS>time-numerosity RS		time-distance RS>distance-numerosity RS		time-numerosity RS>distance-numerosity RS	
		t_{23}	p_{corr}	t_{23}	p_{corr}	t_{23}	p_{corr}
IPS, postcentral gyrus, inferior parietal lobule	right	7.0	<0.001	6.4	<0.001	−0.5	>0.5
IFG	right	4.2	<0.001	2.6	.025	−2.2	.06
	left	5.5	<0.001	1.1	.35	−3.3	.006
hMT+, fusiform gyrus, inferior occipital gyrus	right	10.2	<0.001	10.8	<0.001	0.5	>0.5
	left	11.3	<0.001	11.1	<0.001	</>0.1	>0.5
lingual gyrus	right	1.2	.34	4.5	<0.001	3.8	.003
	left	1.4	.26	5.9	<0.001	3.1	.010
middle occipital gyrus	right	7.1	<0.001	7.3	<0.001	−0.5	>0.5
postcentral gyrus	right	3.5	.004	3.4	.006	−1.3	.28
superior medial gyrus		3.1	.010	0.6	>0.5	−3.6	.004
paracentral gyrus		−0.6	>0.5	0.3	>0.5	0.9	.50

a longer distance in the same time requires higher speed). This situation is different for the time-on-distance effect. If the illusory increase of an actually constant distance is driven by an increase in speed (rather than by an increase in travel time), then we would expect a reversed (i.e., a negative) relation between travel time and perceived traveled distance, because, given a constant distance, travel time correlates negatively with speed (a longer travel time for the same distance can only be achieved by reducing speed). This is the pattern that we found the present study.

In line with this interpretation that the interference between travel time and traveled distance is mediated by speed, many studies reported a positive relation between traveled distance and perceived travel time, while no or a negative relation was found between travel time and perceived distance (Frenz and Lappe, 2005; Herman et al., 1984; Montello, 1997; Riemer et al., 2018; van Rijn, 2014; but see Cohen et al., 1963).

The symmetry or asymmetry of cross-dimensional interferences is also a matter of debate in the literature on the interaction between time and space perception in general (Cai and Connell, 2015; Casasanto and Boroditsky, 2008; Riemer et al., 2018) .[5] Many studies report an asymmetrical relationship, with time being significantly more affected by space than vice versa (Bottini and Casasanto, 2013; Casasanto and Boroditsky, 2008; Merritt et al., 2010). Others have argued that the apparent asymmetry reflects a confound of spatial stimuli being more salient than temporal stimuli (Cai and Connell, 2015; Homma and Ashida, 2015) or of spatial magnitudes being presented instantaneously without continuous accumulation (which is impossible for the dimension of time; Lambrechts et al., 2013; Riemer, 2015). Is has also been argued that the time-space asymmetry is an epiphenomenon of the fact that the processing of spatial information is behaviorally more relevant than the processing of temporal contingencies (Riemer et al., 2018). Indeed, studies reporting an absence or a relative insignificance of an interference from time on space (e.g., Bottini and Casasanto, 2013; Casasanto et al., 2010; Casasanto and Boroditsky, 2008; Gijssels et al., 2013; Merritt et al., 2010) are accompanied by many other studies demonstrating a time-on-space effect of a comparable size as the space-on-time effect (e.g., Cai and Connell, 2015; Homma and Ashida, 2015; Lambrechts et al., 2013; Lourenco and Longo, 2010; Experiment 1 in Riemer et al., 2018).

A critical difference between the studies supporting and disproving the idea of an asymmetrical time-space interference seems to lie in the involvement of a speed component. Either no or a reversed effect of time on space was found in studies using dynamic stimuli, in which time and space dimensions are connected via some factor of speed (moving objects in Bottini and Casasanto, 2013; growing lines in Gijssels et al., 2013; accumulating surface in Martin et al., 2017; self-motion in the present study), whereas the majority of studies using static stimuli show a positive effect of time on space (e.g., Cai and Connell, 2015; Homma and Ashida, 2015; Lourenco and Longo, 2010; Experiment 1 in Riemer et al., 2018; but see Experiment 6 in Casasanto and Boroditsky, 2008).

Hence, on a more general level, the asymmetric interference between travel time and traveled distance found in the present and in other studies reinforce the idea that time-space interferences are governed by the factor of speed (Storch and Zimmermann, 2019). As long as temporal and spatial stimuli are presented statically (i.e., without a speed component) a symmetric interference is observed. Space is influenced by time to a comparable degree as vice versa. But as soon as a speed component is introduced, it governs the time-space interference. Increases in speed lead to increases in temporal and spatial estimates. And with respect to the direct relation between time and space, this results in a positive relationship between actual spatial distance and perceived time, and in a negative relationship between actual time and perceived spatial distance.

Neuroimaging studies in humans and single cell recordings in animals suggest an involvement of right-hemispheric parietal and frontal brain regions in the processing of temporal, spatial and numerical magnitudes (Bueti and Walsh, 2009; Leon and Shadlen, 2003; Nieder et al., 2006; Riemer et al., 2016; Skagerlund et al., 2016; Walsh, 2003). These findings led to the assumption that these areas contain a dimension-unspecific magnitude system (Bueti and Walsh, 2009; Walsh, 2003). However, the fact that different magnitudes are processed in common areas does not necessarily mean that these areas are directly involved in the interference across those magnitudes. The results of the present study are unclear with respect to this issue. While representational similarity in the right IPS was correlated with the time-on-distance effect, we did not find a significant correlation for the reversed distance-on-time effect. This result shows that the right IPS in principle is involved in cross-dimensional interferences between time and distance, but it seems that this involvement depends on the direction of interference. Based on the present study we cannot explain this direction dependency. However, it highlights an issue that has been largely unaddressed to date. Many studies investigated either the asymmetry of time-space interferences (e.g., whether time is more influenced by space than vice versa; Cai and Connell, 2015; Casasanto and Boroditsky, 2008; Riemer et al., 2018) or the role of the IPS for time-space interferences (e.g., Magnani et al., 2010; Oliveri et al., 2009; Riemer et al., 2016). The present study suggests that

[5] It is important to distinguish the interference between travel time and traveled distance (involving a speed component) from the interference between time and space in general (usually not involving a speed component).

it might be advisable to combine these research questions and to clarify whether the role of the IPS depends on the direction of influence.

Using transcranial magnetic stimulation, Hayashi et al. (2013) suggested that the right inferior frontal gyrus (IFG) is specifically involved in the decision phase of magnitude comparison, while the right intraparietal cortex modulates the degree of cross-dimensional interference. This interpretation is supported by our findings. Representational similarity in the right IPS correlated with the interference from time on distance. Independent of the strength of this interference effect, we found a common activation of the right IFG in all trials requiring continuous accumulation of a magnitude (i.e., time, distance and numerosity trials; see univariate fMRI results in Section 3.2.1). In addition to the study by Hayashi et al. (2013), our results show that the right IFG is already recruited during the accumulation phase, that is, before a categorical decision is made.

An important question relates to the cognitive level at which cross-dimensional interferences between travel time and traveled distance occur. There are three possible processing stages. First, interference can emerge at the level of stimulus processing. For example, when accumulating temporal information during a time trial, the accumulation process might be contorted by an automatic parallel processing of spatial distance, which ultimately would result in a distorted input signal. Second, at the representational level. Assuming a veridical processing of all parameters (i.e., time, distance and speed), the neuronal representation of these interdependent magnitudes might overlap to some extent (Pinel et al., 2004). For example, parietal brain regions are sensitive to information from various magnitudes including time, space, numerosity and movement speed (Britten, 2008; Cona et al., 2021; Gijssels et al., 2013; Parkinson et al., 2014; Walsh, 2003), and Pinel et al. (2004) reported that the interference between two magnitudes scaled with the size of the respective overlapping neuronal representations. Third, at the level of response selection. Being exposed to a low value of a task-irrelevant magnitude might prime a congruent response, even if the task requires judgments with respect to a different magnitude. In this case, cross-dimensional interference would reflect mere response biases.

This third possibility is disproved by the fact that an interference effect did neither appear between travel time and numerosity nor between traveled distance and numerosity, although the decision between the responses 'less' and 'more' was equal for time, distance and numerosity trials. Instead, the results of the present study are in favor of the first and the second possibility. Evidence for the interpretation that the interference between travel time and traveled distance emerges during the accumulation process or at the representational level is provided by the finding that individual representational similarity during the accumulation of time and distance information in speed-sensitive brain regions (hMT+ and IPS) is correlated with the strength of the interference effect: More similar activation patterns lead to a stronger influence of traveled distance on perceived travel time (or a stronger influence of travel time on perceived traveled distance, respectively; cf. Fig. 4). Moreover, the absence of interference between numerosity and either time or distance in the present study matches the observation that, for all regions showing higher activity during magnitude accumulation, both time-numerosity and distance-numerosity representational similarity was considerably smaller than the representational similarity between time and distance (Fig. 5 and Table 2).

A limitation of the present study is that area hMT+ was not defined on the basis of a functional localizer, as is typically done in studies on motion perception (e.g., Kamitani and Tong, 2006; van Kemenade et al., 2014). Instead, we used an atlas-based approach (Amunts et al., 2007; Eickhoff et al., 2005), in which hMT+ was defined based on cytoarchitectonic properties (Malikovic et al., 2006) to anatomically characterize the observed clusters. Although Wilms et al. (2005) observed a reasonable correspondence of this cytoarchitectonic map with functionally defined hMT+, implementing a functional localizer would have reduced the influence of individual variability in hMT+ location.

The absence of numerosity-related interference effects suggests that numerosity either was not automatically processed (in time and distance trials) or that this process did not interfere with time and distance accumulation. It should be noted that the absence of numerosity-related interference effects in the present study contrasts with many previous reports (e.g., Cicchini et al., 2016; Dormal and Pesenti, 2013; Hayashi et al., 2013; Schlichting et al., 2018). A possible explanation for this inconsistency lies in the design of our study. The relation between travel time and traveled distance is very obvious. Although time and distance can be decoupled by varying the speed of motion (e.g., Robinson and Wiener, 2021), it usually does take more time to walk a longer distance. Such a naturalistic relationship towards either time or distance is less evident for the abstract concept of numerosity, and this might have reduced the numerosity-related interference effects in our study. A potential way to test this assumption consists in a more naturalistic implementation of the numerosity dimension in future studies. For example, participants could be asked to estimate the number of cars parked at the sidewalks, because the idea of cars has a more obvious relation both to spatial distance (i.e., car length) and to travel time (i.e., it takes time to walk past a car) than the more abstract idea of dots flashing on the ground.

5. Conclusion

In the present study, we show that the strength of cross-dimensional interference effects between travel time and traveled distance correlates with representational similarity in speed-sensitive brain regions. The effect of distance on time was associated with higher representational similarity in left area hMT+ and fusiform gyrus, and the effect of time on distance was associated with higher representational similarity in the right IPS. Together with the finding of an opposite direction for the interference from distance on time and the interference from time on distance (which would be expected under the assumption that the perception of speed is the modulating factor), these results support the view that the asymmetric interference between travel time and traveled distance is mediated by neuronal computations in speed-sensitive parietal and extrastriate areas.

6. Significance statement

Many studies show that the perception of travel time and of traveled distance interfere with each other. Representations of movement speed provide a possible mechanism for this interference, but to date the role of speed representations for time-distance interference has not been investigated. The present study employs a combined fMRI-behavioral paradigm to investigate the relation between behavioral interference between travel time and distance and neuronal representations of movement speed.

Using representational similarity analysis (RSA), we show that behavioral measures for time-distance interference correlate with greater representational similarity in speed-sensitive brain regions such as the intraparietal sulcus and area hMT+. To the best of our knowledge, this is the first evidence connecting time-distance interference effects at the behavioral level with the amount of representational similarity at the neuronal level.

Declaration of Competing Interest

The authors declare no competing financial interests.

Credit authorship contribution statement

Martin Riemer: Conceptualization, Methodology, Funding acquisition, Data curation, Writing – review & editing. **Johannes Achtzehn:** Methodology, Data curation, Writing – review & editing. **Esther Kuehn:** Conceptualization, Methodology, Data curation, Writing – review &

editing. **Thomas Wolbers:** Conceptualization, Methodology, Data curation, Writing – review & editing.

Acknowledgements

This study was supported by the European Social Funds (ESF) (Sachsen-Anhalt Wissenschaft Spitzenforschung/Synergien: AGETIME) and a research grant of the German Research Foundation (DFG) (project number: 452179073). Funding sources had no direct involvement in the study.

Data and Code Availability Statement

The datasets generated during and/or analysed during the current study are available at GitHub: https://github.com/jAchtzehn/timePath.

The GitHub repository contains all code that was used to analyze both behavioural (timePath/behavioural/) and imaging (timePath/mri/) data.

References

Aguirre, G.K., 2007. Continuous carry-over designs for fMRI. Neuroimage 35 (4), 1480–1494. doi:10.1016/j.neuroimage.2007.02.005.

Amunts, K., Schleicher, A., Zilles, K., 2007. Cytoarchitecture of the cerebral cortex—More than localization. Neuroimage 37 (4), 1061–1065. doi:10.1016/j.neuroimage.2007.02.037.

Andersson, J.L.R., Skare, S., Ashburner, J., 2003. How to correct susceptibility distortions in spin-echo echo-planar images: application to diffusion tensor imaging. Neuroimage 20 (2), 870–888. doi:10.1016/S1053-8119(03)00336-7.

Benjamini, Y., Hochberg, Y., 1995. Controlling the false discovery rate: A practical and powerful approach to multiple testing 57 (1), 289–300.

Bottini, R., Casasanto, D., 2013. Space and time in the child's mind: metaphoric or ATOMic? Front. Psychol. 4. doi:10.3389/fpsyg.2013.00803.

Bremmer, F., Lappe, M., 1999. The use of optical velocities for distance discrimination and reproduction during visually simulated self motion. Exp. Brain Res. 127 (1), 33–42. doi:10.1007/s002210050771.

Britten, K.H., 2008. Mechanisms of self-motion perception. Annu. Rev. Neurosci. 31 (1), 389–410. doi:10.1146/annurev.neuro.29.051605.112953.

Bueti, D., Walsh, V., 2009. The parietal cortex and the representation of time, space, number and other magnitudes. Philos. Trans. R. Soc. B: Biol. Sci. 364 (1525), 1831–1840. doi:10.1098/rstb.2009.0028.

Cai, Z.G., Connell, L., 2015. Space–time interdependence: evidence against asymmetric mapping between time and space. Cognition 136, 268–281. doi:10.1016/j.cognition.2014.11.039.

Casasanto, D., Boroditsky, L., 2008. Time in the mind: using space to think about time. Cognition 106 (2), 579–593. doi:10.1016/j.cognition.2007.03.004.

Casasanto, D., Fotakopoulou, O., Boroditsky, L., 2010. Space and time in the child's mind: evidence for a cross-dimensional asymmetry. Cogn. Sci. 34 (3), 387–405. doi:10.1111/j.1551-6709.2010.01094.x.

Chrastil, E.R., Sherrill, K.R., Hasselmo, M.E., Stern, C.E., 2015. There and back again: hippocampus and retrosplenial cortex track homing distance during human path integration. J. Neurosci. 35 (46), 15442–15452. doi:10.1523/JNEUROSCI.1209-15.2015.

Cicchini, G.M., Anobile, G., Burr, D.C., 2016. Spontaneous perception of numerosity in humans. Nat. Commun. 7 (1), 12536. doi:10.1038/ncomms12536.

Cohen, J., Cooper, P., Ono, A., 1963. The hare and the tortoise: a study of the tau-effect in walking and running. Acta Psychol. (Amst) 21, 387–393. doi:10.1016/0001-6918(63)90061-1.

Cona, G., Wiener, M., Scarpazza, C., 2021. From ATOM to GradiATOM: cortical gradients support time and space processing as revealed by a meta-analysis of neuroimaging studies. Neuroimage 224, 117407. doi:10.1016/j.neuroimage.2020.117407.

Cox, R.W., 1996. AFNI: software for analysis and visualization of functional magnetic resonance neuroimages. Comput. Biomed. Res. 29 (3), 162–173. doi:10.1006/cbmr.1996.0014.

Dale, A.M., Fischl, B., Sereno, M.I., 1999. Cortical surface-based analysis: I. Segmentation and surface reconstruction. Neuroimage 9 (2), 179–194. doi:10.1006/nimg.1998.0395.

Dormal, V., Pesenti, M., 2013. Processing numerosity, length and duration in a three-dimensional Stroop-like task: towards a gradient of processing automaticity? Psychol. Res. 77 (2), 116–127. doi:10.1007/s00426-012-0414-3.

Duffy, C.J., Wurtz, R.H., 1997. Medial superior temporal area neurons respond to speed patterns in optic flow. J Neurosci 17 (8), 2839–2851. doi:10.1523/JNEUROSCI.17-08-02839.1997.

Eickhoff, S.B., Stephan, K.E., Mohlberg, H., Grefkes, C., Fink, G.R., Amunts, K., Zilles, K., 2005. A new SPM toolbox for combining probabilistic cytoarchitectonic maps and functional imaging data. Neuroimage 25 (4), 1325–1335. doi:10.1016/j.neuroimage.2004.12.034.

Eklund, A., Nichols, T.E., Knutsson, H., 2016. Cluster failure: why fMRI inferences for spatial extent have inflated false-positive rates. Proc. Natl. Acad. Sci. 113 (28), 7900–7905. doi:10.1073/pnas.1602413113.

Esteban, O., Markiewicz, C.J., Blair, R.W., Moodie, C.A., Isik, A.I., Erramuzpe, A., Kent, J.D., Goncalves, M., DuPre, E., Snyder, M., Oya, H., Ghosh, S.S., Wright, J., Durnez, J., Poldrack, R.A., Gorgolewski, K.J., 2019. fMRIPrep: a robust preprocessing pipeline for functional MRI. Nat. Methods 16 (1), 111–116. doi:10.1038/s41592-018-0235-4.

Faul, F., Erdfeder, E., Lang, A.-G., Buchner, A., 2007. G*Power 3: a flexible statistical power analysis program for the social, behavioral, and biomedical sciences. Behav. Res. Methods 39 (2), 175–191. doi:10.3758/BF03193146.

Fonov, V., Evans, A., McKinstry, R., Almli, C., Collins, D., 2009. Unbiased nonlinear average age-appropriate brain templates from birth to adulthood. Neuroimage 47, S102. doi:10.1016/S1053-8119(09)70884-5.

Frenz, H., Lappe, M., 2005. Absolute travel distance from optic flow. Vision Res. 45 (13), 1679–1692. doi:10.1016/j.visres.2004.12.019.

Gijssels, T., Bottini, R., Rueschemeyer, S.-A., Casasanto, D., 2013. Space and time in the parietal cortex: FMRI Evidence for a meural asymmetry. In: Proceedings of the 35th Annual Meeting of the Cognitive Science Society, pp. 495–500 *CogSci 2013*ppCognitive Science Society.

Gorgolewski, K., Burns, C.D., Madison, C., Clark, D., Halchenko, Y.O., Waskom, M.L., Ghosh, S.S., 2011. Nipype: a flexible, lightweight and extensible neuroimaging data processing framework in python. Front. Neuroinf. 5. doi:10.3389/fninf.2011.00013.

Hanke, M., Halchenko, Y.O., Sederberg, P.B., Hanson, S.J., Haxby, J.V., Pollmann, S., 2009. PyMVPA: a python toolbox for multivariate pattern analysis of fMRI data. Neuroinformatics 7 (1), 37–53. doi:10.1007/s12021-008-9041-y.

Hayashi, M.J., Kanai, R., Tanabe, H.C., Yoshida, Y., Carlson, S., Walsh, V., Sadato, N., 2013. Interaction of numerosity and time in prefrontal and parietal cortex. J. Neurosci. 33 (3), 883–893. doi:10.1523/JNEUROSCI.6257-11.2013.

He, S., Cohen, E.R., Hu, X., 1998. Close correlation between activity in brain area MT/V5 and the perception of a visual motion aftereffect. Curr. Biol. 8 (22), 1215–1218. doi:10.1016/S0960-9822(07)00512-X.

Herman, J.F., Roth, S.F., Norton, L.M., 1984. Time and distance in spatial cognition development. Int. J. Behav. Dev. 7 (1), 35–51. doi:10.1177/016502548400700103.

Homma, C.T., Ashida, H., 2015. What makes space-time interactions in human vision asymmetrical? Front. Psychol. 6. doi:10.3389/fpsyg.2015.00756.

Hutton, C., Bork, A., Josephs, O., Deichmann, R., Ashburner, J., Turner, R., 2002. Image distortion correction in fMRI: a quantitative evaluation. Neuroimage 16 (1), 217–240. doi:10.1006/nimg.2001.1054.

Jenkinson, M., Bannister, P., Brady, M., Smith, S., 2002. Improved optimization for the robust and accurate linear registration and motion correction of brain images. Neuroimage 17 (2), 825–841. doi:10.1006/nimg.2002.1132.

Kamitani, Y., Tong, F., 2006. Decoding seen and attended motion directions from activity in the human visual cortex. Curr. Biol. 16 (11), 1096–1102. doi:10.1016/j.cub.2006.04.003.

Klein, A., Ghosh, S.S., Bao, F.S., Giard, J., Häme, Y., Stavsky, E., Lee, N., Rossa, B., Reuter, M., Chaibub Neto, E., Keshavan, A., 2017. Mindboggling morphometry of human brains. PLoS Comput. Biol. 13 (2), e1005350. doi:10.1371/journal.pcbi.1005350.

Kuehn, E., Perez-Lopez, M.B., Diersch, N., Döhler, J., Wolbers, T., Riemer, M., 2018. Embodiment in the aging mind. Neurosci. Biobehav. Rev. 86, 207–225. doi:10.1016/j.neubiorev.2017.11.016.

Lakens, D., 2013. Calculating and reporting effect sizes to facilitate cumulative science: a practical primer for t-tests and ANOVAs. Front. Psychol. 4. doi:10.3389/fpsyg.2013.00863.

Lambrechts, A., Walsh, V., van Wassenhove, V., 2013. Evidence accumulation in the magnitude system. PLoS One 8 (12), e82122. doi:10.1371/journal.pone.0082122.

Leon, M.I., Shadlen, M.N., 2003. Representation of time by neurons in the posterior parietal cortex of the macaque. Neuron 38 (2), 317–327. doi:10.1016/S0896-6273(03)00185-5.

Livesey, A.C., Wall, M.B., Smith, A.T., 2007. Time perception: manipulation of task difficulty dissociates clock functions from other cognitive demands. Neuropsychologia 45 (2), 321–331. doi:10.1016/j.neuropsychologia.2006.06.033.

Lorenz, S., Weiner, K.S., Caspers, J., Mohlberg, H., Schleicher, A., Bludau, S., Eickhoff, S.B., Grill-Spector, K., Zilles, K., Amunts, K., 2015. Two new cytoarchitectonic areas on the human mid-fusiform gyrus. Cereb. Cortex doi:10.1093/cercor/bhv225, bhv225.

Lourenco, S.F., Longo, M.R., 2010. General magnitude representation in human infants. Psychol. Sci. 21 (6), 873–881. doi:10.1177/0956797610370158.

Maaß, S., Wolbers, T., van Rijn, H., Riemer, M., 2022. Temporal context effects are associated with cognitive status in advanced age. Psychol. Res. 86 (2), 512–521. doi:10.1007/s00426-021-01502-9.

Magnani, B., Oliveri, M., Mangano, G.R., Frassinetti, F., 2010. The role of posterior parietal cortex in spatial representation of time: a TMS study. Behav. Neurol. 23 (4), 213–215. doi:10.1155/2010/282950.

Malikovic, A., Amunts, K., Schleicher, A., Mohlberg, H., Eickhoff, S.B., Wilms, M., Palomero-Gallagher, N., Armstrong, E., Zilles, K., 2006. Cytoarchitectonic analysis of the human extrastriate cortex in the region of V5/MT+: a probabilistic, stereotaxic map of area hOc5. Cereb. Cortex 17 (3), 562–574. doi:10.1093/cercor/bhj181.

Marcus, D.S., Wang, T.H., Parker, J., Csernansky, J.G., Morris, J.C., Buckner, R.L., 2007. Open Access Series of Imaging Studies (OASIS): cross-sectional MRI data in young, middle aged, nondemented, and demented older adults. J. Cogn. Neurosci. 19 (9), 1498–1507. doi:10.1162/jocn.2007.19.9.1498.

Martin, B., Wiener, M., van Wassenhove, V., 2017. A Bayesian perspective on accumulation in the magnitude system. Sci. Rep. 7 (1), 630. doi:10.1038/s41598-017-00680-0.

Martinez-Trujillo, J.C., Cheyne, D., Gaetz, W., Simine, E., Tsotsos, J.K., 2007. Activation of area MT/V5 and the right inferior parietal cortex during the discrimination of transient direction changes in translational motion. Cereb. Cortex 17 (7), 1733–1739. doi:10.1093/cercor/bhl084.

Martinez-Trujillo, J.C., Tsotsos, J.K., Simine, E., Pomplun, M., Wildes, R., Treue, S., Heinze, H.-J., Hopf, J.-M., 2005. Selectivity for speed gradients in human area MT/V5. Neuroreport 16 (5), 435–438. doi:10.1097/00001756-200504040-00004.

Merritt, D.J., Casasanto, D., Brannon, E.M., 2010. Do monkeys think in metaphors? Representations of space and time in monkeys and humans. Cognition 117 (2), 191–202. doi:10.1016/j.cognition.2010.08.011.

Mioni, G., Román-Caballero, R., Clerici, J., Capizzi, M., 2021. Prospective and retrospective timing in mild cognitive impairment and Alzheimer's disease patients: a systematic review and meta-analysis. Behav. Brain Res. 410, 113354. doi:10.1016/j.bbr.2021.113354.

Montello, D.R. (1997). The perception and cognition of environmental distance: direct sources of information. In *Spatial information theory: A theoretical basis for GIS* (pp. 297–311). Springer-Verlag.

Mumford, J.A., Turner, B.O., Ashby, F.G., Poldrack, R.A., 2012. Deconvolving BOLD activation in event-related designs for multivoxel pattern classification analyses. Neuroimage 59 (3), 2636–2643. doi:10.1016/j.neuroimage.2011.08.076.

Nieder, A., Diester, I., Tudusciuc, O., 2006. Temporal and spatial enumeration processes in the primate parietal cortex. Science 313 (5792), 1431–1435. doi:10.1126/science.1130308.

Oliveri, M., Koch, G., Salerno, S., Torriero, S., Gerfo, E.L., Caltagirone, C., 2009. Representation of time intervals in the right posterior parietal cortex: implications for a mental time line. Neuroimage 46 (4), 1173–1179. doi:10.1016/j.neuroimage.2009.03.042.

Parkinson, C., Liu, S., Wheatley, T., 2014. A common cortical metric for spatial, temporal, and social distance. J. Neurosci. 34 (5), 1979–1987. doi:10.1523/JNEUROSCI.2159-13.2014.

Pinel, P., Piazza, M., Le Bihan, D., Dehaene, S., 2004. Distributed and overlapping cerebral representations of number, size, and luminance during comparative judgments. Neuron 41 (6), 983–993. doi:10.1016/S0896-6273(04)00107-2.

Richter, M., Amunts, K., Mohlberg, H., Bludau, S., Eickhoff, S.B., Zilles, K., Caspers, S., 2019. Cytoarchitectonic segregation of human posterior intraparietal and adjacent parieto-occipital sulcus and its relation to visuomotor and cognitive functions. Cereb. Cortex 29 (3), 1305–1327. doi:10.1093/cercor/bhy245.

Riemer, M., 2015. Psychophysics and the anisotropy of time. Conscious. Cogn. 38, 191–197. doi:10.1016/j.concog.2015.06.007.

Riemer, M., Diersch, N., Bublatzky, F., Wolbers, T., 2016. Space, time, and numbers in the right posterior parietal cortex: differences between response code associations and congruency effects. Neuroimage 129, 72–79. doi:10.1016/j.neuroimage.2016.01.030.

Riemer, M., Hölzl, R., Kleinböhl, D., 2014. Interrelations between the perception of time and space in large-scale environments. Exp. Brain Res. 232 (4), 1317–1325. doi:10.1007/s00221-014-3848-6.

Riemer, M., Shine, J.P., Wolbers, T., 2018. On the (a)symmetry between the perception of time and space in large-scale environments. Hippocampus 28 (8), 539–548. doi:10.1002/hipo.22954.

Riemer, M., Wolbers, T., van Rijn, H., 2021. Age-related changes in time perception: the impact of naturalistic environments and retrospective judgements on timing performance. Q. J. Exp. Psychol. 74 (11), 2002–2012. doi:10.1177/17470218211023362.

Robinson, E.M., Wiener, M., 2021. Dissociable neural indices for time and space estimates during virtual distance reproduction. Neuroimage 226, 117607. doi:10.1016/j.neuroimage.2020.117607.

Scheperjans, F., Eickhoff, S.B., Homke, L., Mohlberg, H., Hermann, K., Amunts, K., Zilles, K., 2008. Probabilistic maps, morphometry, and variability of cytoarchitectonic areas in the human superior parietal cortex. Cereb. Cortex 18 (9), 2141–2157. doi:10.1093/cercor/bhm241.

Schlichting, N., de Jong, R., van Rijn, H., 2018. Robustness of individual differences in temporal interference effects. PLoS One 13 (8), e0202345. doi:10.1371/journal.pone.0202345.

Schütt, H.H., Harmeling, S., Macke, J.H., & Wichmann, F.A. (2016). Painfree and accurate Bayesian estimation of psychometric functions for (potentially) overdispersed data. *Vision Research*, 122, 105–123. https://doi.org/10.1016/j.visres.2016.02.002

Siegel, R., 1997. Analysis of optic flow in the monkey parietal area 7a. Cereb. Cortex 7 (4), 327–346. doi:10.1093/cercor/7.4.327.

Skagerlund, K., Karlsson, T., Träff, U., 2016. Magnitude processing in the brain: an fMRI study of time, space, and numerosity as a shared cortical system. Front. Hum. Neurosci. 10. doi:10.3389/fnhum.2016.00500.

Stangl, M., Kanitscheider, I., Riemer, M., Fiete, I., Wolbers, T., 2020. Sources of path integration error in young and aging humans. Nat. Commun. 11 (1), 2626. doi:10.1038/s41467-020-15805-9.

Storch, D., Zimmermann, E., 2019. The effect of space on subjective time is mediated by apparent velocity. J. Vision 19 (14), 19. doi:10.1167/19.14.19.

Taube, J.S., 2007. The head direction signal: origins and sensory-motor integration. Annu. Rev. Neurosci. 30 (1), 181–207. doi:10.1146/annurev.neuro.29.051605.112854.

Tregellas, J.R., Davalos, D.B., Rojas, D.C., 2006. Effect of task difficulty on the functional anatomy of temporal processing. Neuroimage 32 (1), 307–315. doi:10.1016/j.neuroimage.2006.02.036.

Turner, B.O., Mumford, J.A., Poldrack, R.A., Ashby, F.G., 2012. Spatiotemporal activity estimation for multivoxel pattern analysis with rapid event-related designs. Neuroimage 62 (3), 1429–1438. doi:10.1016/j.neuroimage.2012.05.057.

Tustison, N.J., Avants, B.B., Cook, P.A., Zheng, Yuanjie, Egan, A., Yushkevich, P.A., Gee, J.C., 2010. N4ITK: improved N3 bias correction. IEEE Trans. Med. Imaging 29 (6), 1310–1320. doi:10.1109/TMI.2010.2046908.

van Kemenade, B.M., Seymour, K., Wacker, E., Spitzer, B., Blankenburg, F., Sterzer, P., 2014. Tactile and visual motion direction processing in hMT+/V5. Neuroimage 84, 420–427. doi:10.1016/j.neuroimage.2013.09.004.

van Rijn, H., 2014. It's time to take the psychology of biological time into account: speed of driving affects a trip's subjective duration. Front. Psychol. 5. doi:10.3389/fpsyg.2014.01028.

Vul, E., Harris, C., Winkielman, P., Pashler, H., 2009. Puzzlingly high correlations in fMRI studies of emotion, personality, and social cognition. Perspect. Psychol. Sci. 4 (3), 274–290. doi:10.1111/j.1745-6924.2009.01125.x.

Walsh, V., 2003. A theory of magnitude: common cortical metrics of time, space and quantity. Trends Cogn. Sci. 7 (11), 483–488. doi:10.1016/j.tics.2003.09.002.

Walther, A., Nili, H., Ejaz, N., Alink, A., Kriegeskorte, N., Diedrichsen, J., 2016. Reliability of dissimilarity measures for multi-voxel pattern analysis. Neuroimage 137, 188–200. doi:10.1016/j.neuroimage.2015.12.012.

Wilms, M., Eickhoff, S.B., Specht, K., Amunts, K., Shah, N.J., Malikovic, A., Fink, G.R., 2005. Human V5/MT+: comparison of functional and cytoarchitectonic data. Anat. Embryol. (Berl.) 210 (5–6), 485–495. doi:10.1007/s00429-005-0064-y.

Wolbers, T., Wiener, J.M., Mallot, H.A., Büchel, C., 2007. Differential recruitment of the hippocampus, medial prefrontal cortex, and the human motion complex during path integration in humans. J. Neurosci. 27 (35), 9408–9416. doi:10.1523/JNEUROSCI.2146-07.2007.

Wurtz, R.H., 1998. Optic flow: a brain region devoted to optic flow analysis? Curr. Biol. 8 (16), R554–R556. doi:10.1016/S0960-9822(07)00359-4.

Zhang, Y., Brady, M., Smith, S., 2001. Segmentation of brain MR images through a hidden Markov random field model and the expectation-maximization algorithm. IEEE Trans. Med. Imaging 20 (1), 45–57. doi:10.1109/42.906424.